Chemical Papers (2021) 75:4035–4044
https://doi.org/10.1007/s11696-021-01589-9

ORIGINAL PAPER

Simple and feasible design of a polymeric nanoparticle for efficient anticancer drug delivery

Yue Zhao[1] · Rui Zhong[1] · Yongqiang Fu[1] · Zhenlin Zhou[1] · Ming Yang[1] · Lina He[1]

Received: 3 December 2020 / Accepted: 5 March 2021 / Published online: 10 April 2021

Abstract

In this paper, we present a simple and feasible drug self-assembled delivery system with pH responsiveness and targeting function for cancer therapy. The drug delivery system is composed of an anticancer drug and an amphiphilic random copolymer based on phenylboronic acid, galactose, and polyethylene glycol monomethyl ether acrylate molecules and achieved through reversible addition–fragmentation chain transfer polymerization. The micelles present targeting function by introducing galactose molecules and show pH sensitivity on the basis of the interactions between phenylboronic acid and galactose molecules. Particle size, transmission electron microscopy, and drug release assays show the pH-responsive behavior of micelles at pH 6.0. Cellular uptake assay demonstrates that micelles can internalize HepG2 cells via receptor-mediated interaction. In addition, the drug-loaded micelles can considerably inhibit cancer cell proliferation as indicated by in vivo antitumor assay. The synthesized micelles may facilitate the development of valid drug delivery systems for cancer therapy.

Keywords Copolymer · Galactose · Phenylboronic acid · Drug delivery system · Anticancer

Introduction

In 2018, cancer led to over 9.6 million deaths worldwide. (Bray et al. 2018) At present, the conventional routes to manage cancer are chemotherapeutic by using conventional anticancer drugs although the conventional drugs present some obvious evident drawbacks (Wang et al. 2017a, 2017b; Alexander et al. 2017). Thus, new methods must be sought to treat this fatal disease.

Much effort has been dedicated in the anticancer field to develop new therapeutic drugs for the treatment of cancers (Zhang et al. 2019, 2017a; Lin et al. 2020) For example, a the drug delivery system, as an effective therapeutic strategy, is widely used for cancer chemotherapy. (Wang et al. 2017b; Koyamatsu et al. 2014; Duan et al. 2016; Gao et al. 2017; Zhang et al. 2017b; Saw et al. 2020) Drug delivery systems, such as silica nanoparticles, (Cheng et al. 2019) lipidosomes, (Liposomes assembled from a dual drug-tailed phospholipid for cancer therapy.Chemistry An Asian Journal2015, 10 (5), 1232. 2015; Arouri et al. 2013) vesicles, (Duan et al. 2013), and amphiphilic polymer nanoparticles, (Cho et al. 2008; Guo et al. 2019), are generally viewed as effective alternatives to conventional small drugs in the treatment of diseases.(Zhang et al. 2017a) For example, Saw et al. investigated a formulation of novel lipid-based nanostructures via simple tuning of lipid combinations. The drug encapsulation tests and in vivo antitumor efficacy revealed that certain lipid nanostructures possessed superior tumor retardation effects (Saw et al. 2020). Among these systems, various stimulus-responsive drug delivery systems receive considerable attention owing to their ability to release their encapsulated drugs in response to specific conditions, (Yao et al. 2016; Li et al. 2018; Pan et al. 2018; Han et al. 2018) such as pH, (Cheng et al. 2017) reactive oxygen species, (Zhang et al. 2018; Chen et al. 2021) temperature, (Li et al. 2018), and enzyme (Zhang et al. 2019). Chen et al. developed redox-responsive nanoparticle encapsulating black phosphorus quantum dots (BPQDs) as a robust photothermal optical coherence tomography agent for cancer theranostics (Chen et al. 2021). The system could rapidly respond to glutathione and effectively release BPQDs and drugs in vitro and in vivo. It also exhibited excellent near-infrared photothermal transduction efficiency and could serve as a novel therapeutic platform with considerably low side effects. Li et al. developed a polypeptide-based block ionomer complex by using a polymer/polypeptide and an anticancer drug (Li et al. 2013). Drug release from this complex was rapid at an acidic pH environment and slow at

✉ Yue Zhao
zhaoyue20201104@sina.com

[1] Guiyang Hospital of Guizhou Aviation Industry Group, Guiyang 550006, Guizhou Province, China

physiological pH. All the results demonstrated that the complex drug delivery systems acting as a valid therapeutic modality in the therapy of solid tumors were a promising vector to deliver anticancer drugs into tumors.

Clinical anticancer drugs generally damage normal tissues owing to the lack of recognition between normal and tumor tissues. Therefore, an efficient drug delivery system should be able to distinguish normal and tumor cells by targeting tumor tissues (An et al. 2015). The superiority of nanoparticles with targeting function can improve drug accumulation in tumor tissues and decrease side toxicity (Cheng et al. 2019; Tan et al. 2018). For example, Zhang developed a programmable drug delivery system based on a composite nanoparticle for enhancing and sensitizing chemotherapy to drug-resistant cancer (Zhang et al. 2019). The nanoparticle composed of a cross-linked chondroitin sulfate hydrogel that could mediate tumor-specific CD44 targeting with induced tumor-specific cytotoxicity. An prepared multifunctional nanoparticles for the tumor-targeted delivery of anticancer drugs via self-assembly of amphiphilic copolymers (An et al. 2015). Galactose was introduced into the multifunctional nanoparticles to target the overexpressed protein, that is asialoglycoprotein receptor, in hepatoma cells (Ashwell and Harford 1982; Hashida et al. 2001).

In the present study, we synthesize an amphiphilic random copolymer based on phenylboronic acid, galactose, and polyethylene glycol monomethyl ether acrylate molecules by reversible addition–fragmentation chain transfer (RAFT) polymerization. The amphiphilic copolymer can self-assemble in a water solution to obtain stable and biocompatible micelles. The copolymer is prepared with one step, which is a simple and feasible design for efficient anticancer drug delivery compared with other anticancer systems. Although it is simple, the system is endowed with targeted and pH-responsive groups to enhance the anticancer effect. The micelles present targeting function by introducing galactose molecules and show pH sensitivity on the basis of the interaction between phenylboronic acid and galactose molecules. Particle size, drug delivery, in vitro cell viability, and anticancer effect are investigated to evaluate the potential use of micelles in cancer therapy.

Experiments

Materials

An amphiphilic random copolymer based on phenylboronic acid, galactose, and polyethylene glycol monomethyl ether acrylate molecules was synthesized via RAFT polymerization. The amphiphilic copolymer could self-assemble in a water solution to generate stable and biocompatible micelles. The introduction of galactose molecules led to the targeting function of the micelles, and the interaction between phenylboronic acid and galactose molecules indicates the pH sensitivity of the micelles. Herein, the potential use of micelles in cancer therapy was evaluated through investigating particle size, drug delivery, in vitro cell viability, and anticancer effect.

Synthesis of 3-acrylamidophenylboronic acid (AAPBA)

AAPBA was synthesized in accordance with a previous method (Lee et al. 2004) 3-Aminophenylboronic acid (1.0 g, 6.44 mmol) and sodium carbonate (1.0 g, 11.9 mmol) were added to a H_2O/tetrahydrofuran mixed solution (9 mL, v/v, 2:1). The mixture was cooled in an ice bath. Acryloyl chloride (1 mL, 12.5 mmol) was added dropwise to the mixed solution under strong stirring for over 0.5 h. The reaction was conducted for another 2 h at 25 °C. The solution was extracted with acetic ether, and the organic phase was concentrated to obtain the dry product. After the crude product was recrystallized twice in hot water (80 mL, 90 °C), the purified AAPBA was obtained.

Synthesis of 3-acrylamidophenylboronic acid (LAMA)

LAMA was prepared following a previously described method (He et al. 2007; Cheng et al. 2012). Lactobionolactone (1.0 g, 2.94 mmol) was added to methanol at 40 °C. After the solution was cooled to 25 °C, 2-aminoethyl methacrylate hydrochloride (2.0 g, 12.08 mmol), triethylamine (2.0 mL), and hydroquinone (0.05 g) were added. The mixture was allowed to react for 5 h, and then, the mixture solution was concentrated and precipitated into an amount of isopropanol. After filtering, washing, and drying, the purified LAMA was obtained.

Synthesis of p(AAPBA-*r*-LAMA)

LAMA (3 mmol, 1.40 g), AAPBA (2 mmol, 0.38 g), AIBN (0.05 mol, 8.2 mg), and S-1-dodecyl-S′-(α,α′-dimethyl-α″-aceticacid) trithiocarbonate (0.1 mmol, 36.42 mg) were added to a Schlenk tube and dissolved in 4 mL of a mixed solution (H_2O/DMF, v/v = 1:3). The tube was immersed with argon for 30 min in an ice bath and kept at 70 °C for 24 h. After the reaction was cooled in the ice bath, a random copolymer was obtained by precipitation in excess methanol acetic ether. The copolymer was simply named P*r*L*r*B.

Preparation of nanoparticle

Water (9 mL) was added dropwise to a mixed solution of H_2O/DMF (1 mL, v/v, 1:3) containing the random copolymer P*r*L*r*B (5 mg) under vigorous stirring. The resultant nanoparticle solution was dialyzed against H_2O for 24 h to remove the organic solvent. The obtained nanoparticle was denoted as NP_{PrLrB}.

Loading drug

DOX (2 mg) and P*r*L*r*B (20 mg) were dissolved in 2 mL of H_2O/DMF (v/v, 1:3) solution. H_2O (8 mL) was dropwise added under vigorous stirring. The resultant nanoparticle solution was dialyzed against H_2O for 24 h to remove the organic solvent. The obtained nanoparticle was denoted as NP_{PrLrB}-DOX.

Drug loading and encapsulation efficiency were measured as follows. After the NP_{PrLrB}-DOX solution (3 mL) was centrifuged at 20 000 rpm for 0.5 h, the supernatant was tested using a UV–vis spectrometer at 485 nm. The amount of DOX was estimated using the following equations:

$$\mathrm{LC}\% = \frac{\text{weight of DOX in NPs}}{\text{weight of NPs}} \times 100\% \quad (1)$$

$$\mathrm{EE}\% = \frac{\text{weight of DOX in NPs}}{\text{weight of total DOX}} \times 100\% \quad (2)$$

Characterization of copolymers and nanoparticle

^{1}H NMR spectra were determined at 25 °C by using a Varian Unity-plus 400 NMR spectrometer. Hydrodynamic size (*D*H) was measured by dynamic light scattering (DLS, Malvern Zetasizer Nano S apparatus). The nanoparticle morphology was observed using a transmission electron microscope (FEI).

In vitro DOX release

Exactly 5 mL of the NP_{PrLrB}-DOX solution was transferred to a dialysis tube (MWCO 3500) and dialyzed under shaking (100 rev/min). The dialysis tube was immersed into 25 mL of PBS buffer (pH 6.0, 7.4, and 7.4 with glucose [1 mg/mL]). At specific time intervals, 1.5 mL of the dialyzed medium was obtained for UV–vis measurement ($\lambda = 485$ nm). Then, 1.5 mL of fresh dialyzed medium was added. Each sample was analyzed in triplicate, and the results were recorded as mean ± standard deviation ($n = 3$).

Cytocompatibility assay

The cytotoxicity of materials was evaluated by cell coculture assay. NIH3T3 and HepG2 cells were cultured in DMEM containing 10% fetal bovine serum, 1% penicillin/streptomycin, and 1% nonessential amino acid. Cells were placed in 5% CO_2/95% air at 37 °C. They were seeded at a density of 10^4 cells/well in a 96-well plate. NP_{PrLrB}-DOX was diluted to different concentrations with the cell culture medium and added to the 96-well plate to replace the primary medium. After incubation for 24 h, a 3[4,5-dimethylthiazol-2-yl]-2,5-diphenylterazolium bromide (MTT) (10 μL) solution was added to each well and incubated for another 4 h. After the medium was discarded, DMSO (150 μL) was added to dissolve the formazane crystals. Optical density was recorded at 492 nm on a microplate reader.

In vitro cellular internalization

NIH3T3 and HepG2 cells were cultured in 24-well plates. After the cells were incubated overnight, they were cocultured with predetermined concentrations of NP_{PrLrB}-DOX. After the cells were cultured for a predetermined time, they were washed treated with PBS (pH 7.4) and 4% paraformaldehyde and stained with 4′,6-diamidino-2-phenylindole (DAPI). Then, the internalization was observed using a fluorescent microscope.

In vivo administration

Male BALB/c nude mice (4 weeks old) were purchased from Beijing HFK Bioscience Co., Ltd. (Beijing, China). All the protocols for animal experiments were performed on the basis of the guidelines of the Council for the Purpose of Control and Supervision of Experiments on Animals, Ministry of Public Health, Government of China.

The nude mice were randomly divided into three groups (five mice per group). After tumor volume reached a mean size of approximately 50 mm^3, PBS buffer (pH 7.4), free DOX, and NP_{PrLrB}-DOX were intravenously injected into the mice on the 18th, 24th, and 28th days, respectively, with a dose of 1 mg of DOX per kg of mouse body weight. The tumor size and body weight were measured at a predetermined time. On the 35th day, the major organs of the mice were

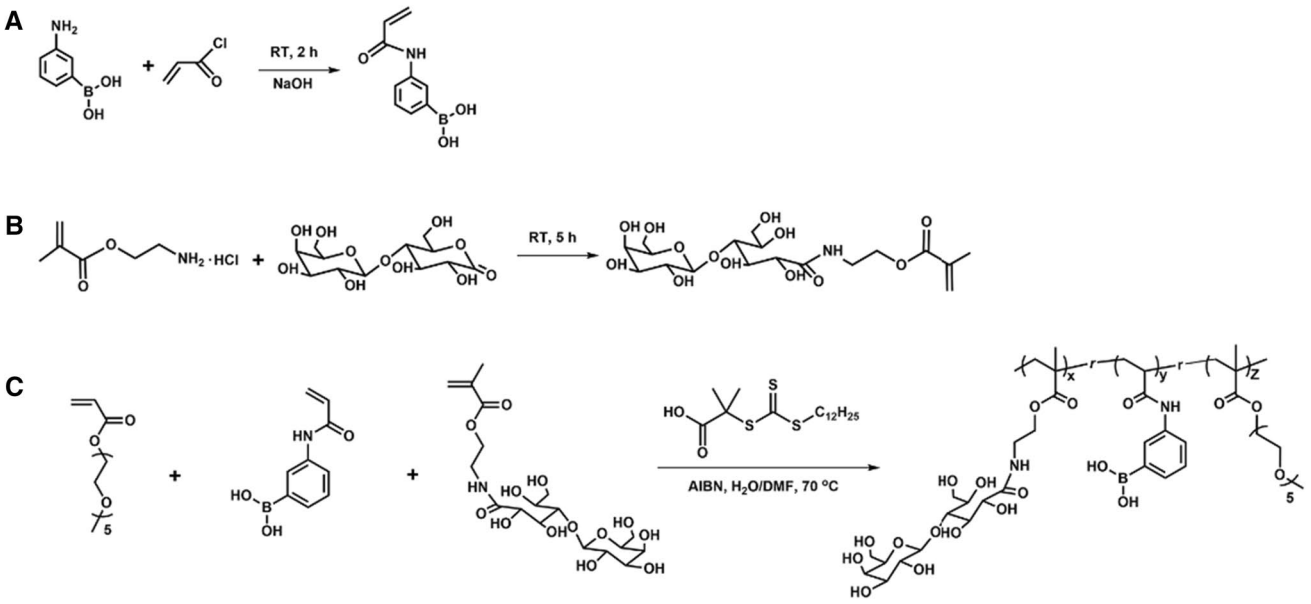

Scheme 1 Synthesis of **a** AAPBA, **b** LAMA and random copolymer p(AAPBA-*r*-LAMA-*r*-PEGMA)

harvested and fixed in 10% neutral buffered formalin for histochemical studies. They were embedded in paraffin, and 4-µm-thick sections were cut and stained with hematoxylin and eosin (H&E). Micrographs were obtained using an optical microscope.

Statistical analysis

All data, expressed as means ± standard deviation, were compared by one-way analysis of Kruskal–Wallis ANOVA. The level of statistical significance was set at $p < 0.05$.

Results and discussion

Synthesis and characterization of random copolymer and nanoparticles

Anticancer materials are generally prepared with complicated procedures to process multiple functions. Herein, we designed and prepared a simple and feasible polymeric system with targeted and pH-responsive functions. The random copolymer p(AAPBA-*r*-LAMA-*r*-PEGMA) (simply denoted as P*r*L*r*B) was synthesized via the RAFT

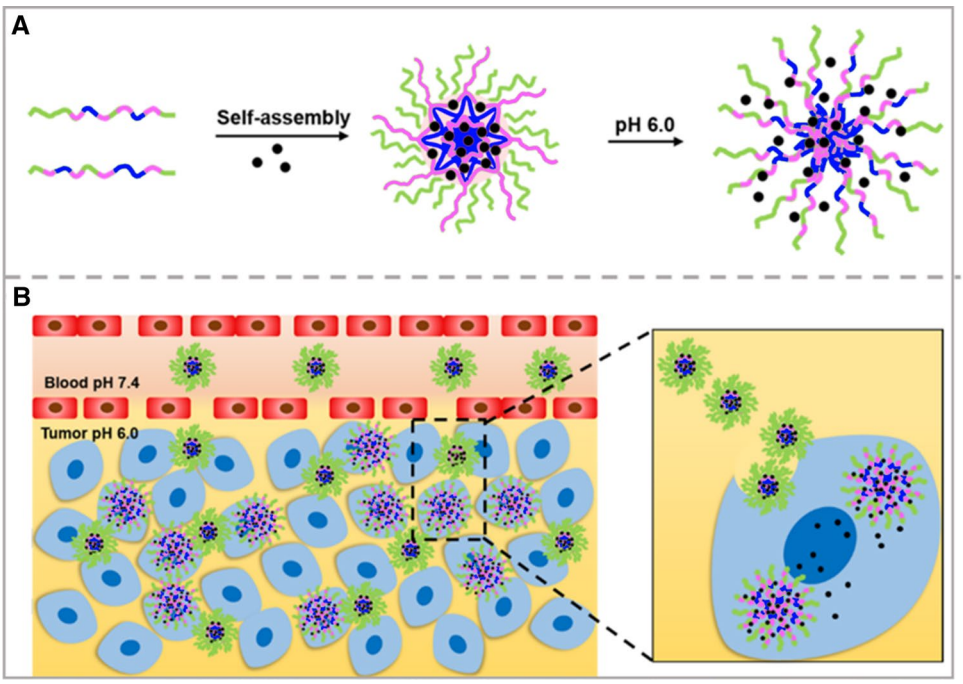

Scheme 2 **a** Self-assembly of P*r*L*r*B copolymer with drugs into nanoparticles and drug release behavior. **b** Interaction of drug-loaded NP_{PrLrB} and tumor cells

polymerization technique with one step (Scheme 1). P*r*L*r*B could self-assemble to form nanoparticles with hydrophilic LAMA corona, LAMA–AAPBA cross-linking layer, and hydrophobic core (Scheme 2). Boronate esters, formed between AAPBA and LAMA, were stable under physiological conditions, but they easily dissociated in an acidic tumor microenvironment (Su et al. 2011; Li et al. 2012) which was beneficial to acid-responding drug release in tumor tissues. Simultaneously, the targeting ligands of LAMA on the nanoparticle surface could be activated to enhance cellular internalization by carbohydrate–protein interactions (An et al. 2015; Lepenies et al. 2013; Fallon and Schwartz 1988; Becker et al. 1995). LAMA had a targeting effect on tumor cells, and its cross-linking layer and core could load drugs for the treatment of diseases. The ^{1}H NMR spectra of AAPBA, LAMA, and P*r*L*r*B are shown in Figs. 1a–c. Compared with the spectra of AAPBA (A) and LAMA (B), the spectrum of P*r*L*r*B retained the resonance signals of phenyl-ring protons and sugar units at 6.0–7.9 and 3.0–3.7 ppm, respectively. The resonance signals assigned to the double-bond protons completely disappeared. New resonance signals appeared at 0.8–1.8 ppm, which were assigned to the main chain protons, as shown in Fig. 1c. These results indicated the successful preparation of the random copolymer P*r*L*r*B and NP_{PrLrB} via a nanoprecipitation technique. Figure 1d shows the hydrodynamic particle size of NP_{PrLrB} of approximately 164.2 nm in a pH 7.4 medium. The nanoparticles exhibited a spherical shape with good dispersion (Fig. 1e). In a pH 6.0 medium, the disassembly of the LAMA–AAPBA cross-linking layer in NP_{PrLrB} led to the decrease in size of approximately 78.2 nm (Fig. 1f). The morphology (Fig. 1g) in pH 6.0 confirmed this result. The disassembly behavior of the

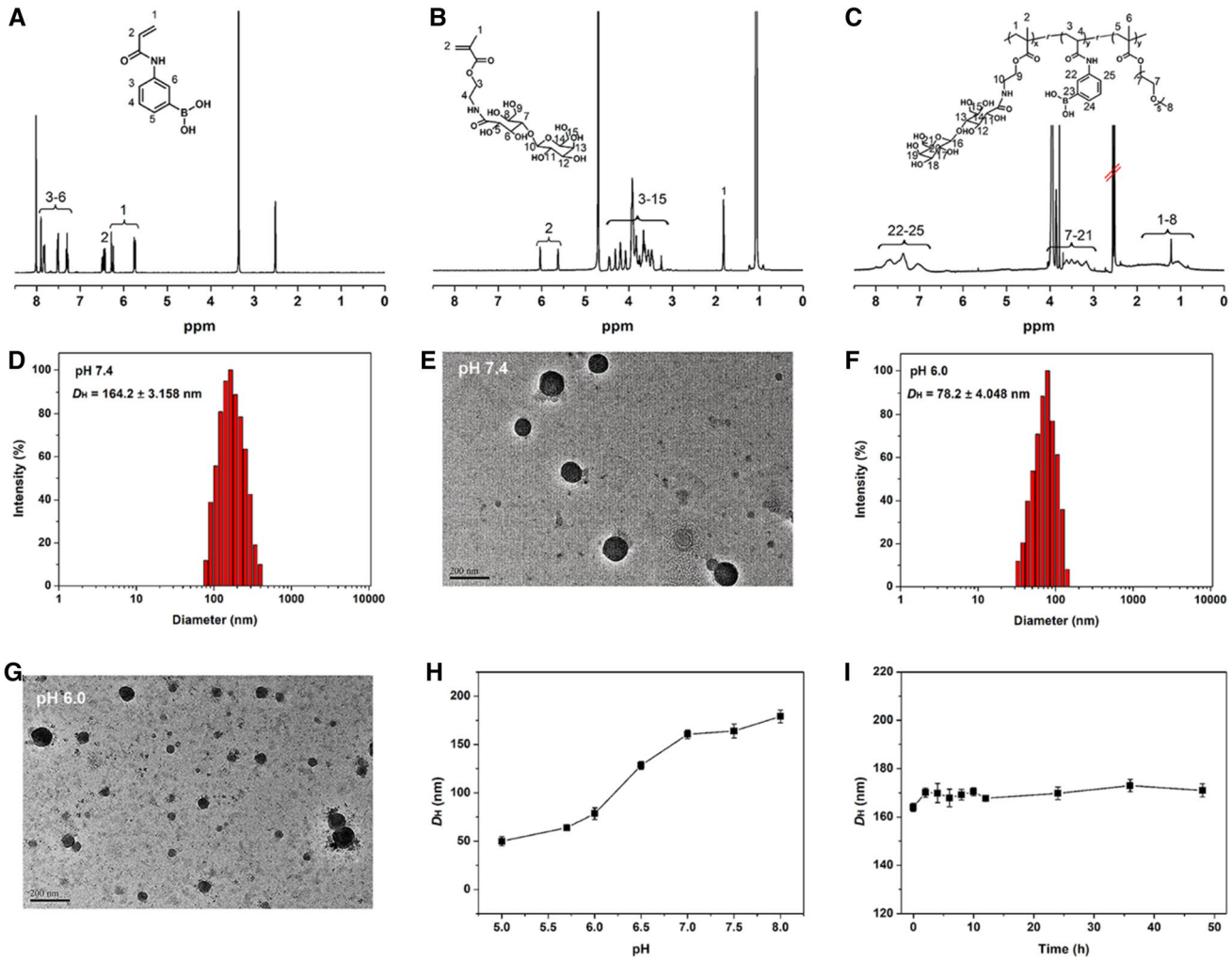

Fig. 1 ^{1}H NMR spectra of **a** AAPBA, **b** LAMA, and **c** P*r*L*r*B. **d** Size of NP_{PrLrB} in a pH 7.4 medium. **e** Morphology of NP_{PrLrB} in a pH 7.4 medium. **f** Size of NP_{PrLrB} in a pH 6.0 medium. **g** Morphology of NP_{PrLrB} in a pH 6.0 medium. **h** Size change of NP_{PrLrB} in different pH media. **i** Stability of NP_{PrLrB} in DMEM with 10% FBS medium

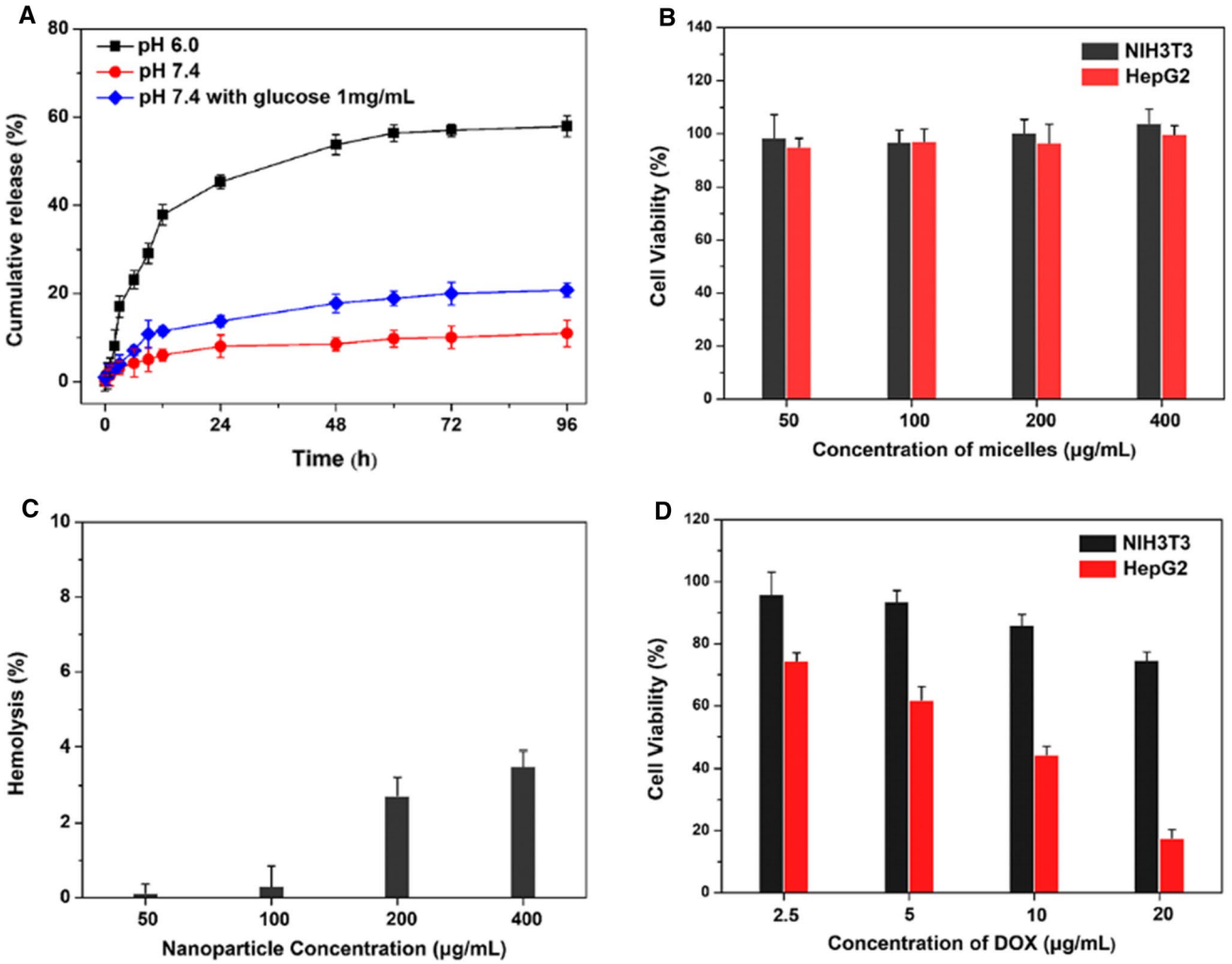

Fig. 2 **a** In vitro DOX release from NP_{PrLrB}-DOX in different media. **b** Cell viability of NIH3T3 and HepG2 cells after being treated with various concentrations of NP_{PrLrB}. **c** Hemolysis of NIH3T3 and HepG2 cells after being treated with various concentrations of NP_{PrLrB}. **d** Cell viability of NIH3T3 and HepG2 cells after being treated with various concentrations of NP_{PrLrB}-DOX ($p < 0.05$)

LAMA–AAPBA (Guo et al. 2019) cross-linking layer is important because it makes the foundation for the drug release in the tumor environment. The size changes in different pH media were measured to evaluate the disassembly behavior of NP_{PrLrB} further. The size of NP_{PrLrB} in an acidic condition was generally smaller than that in a neutral or alkaline condition (Fig. 1h). The stability of NP_{PrLrB} was studied by measuring its size in DMEM with 10% FBS. The result in Fig. 1i shows that NP_{PrLrB} can be kept stable for 2 days. The stability of the nanoparticle in a cell culture medium is important for its use in cell and animal assays.

Drug loading and cellular assays of NP_{PrLrB}-DOX

Herein, DOX was used as a model chemotherapeutic agent. DOX was loaded into NP_{PrLrB} with LC of 9.7% and EE of 71.3%. In vitro release of DOX was tested in different media, and the results are shown in Fig. 2a. To mimic physiological (e.g., in blood circulation) and tumor environments, three release media, that is, pH 7.4, pH 7.4 with glucose (1 mg/mL), and pH 6.0, were used. In Fig. 2a, the DOX cumulative release from NP_{PrLrB}-DOX at pH 7.4, pH 7.4 with glucose, and pH 6.0 was 10.9%, 20.7%, and 57.9%, respectively, over 96 h. The higher release in pH 7.4 with glucose than that in pH 7.4 might have resulted from the local swelling of AAPBA core on the basis of the conjugation between AAPBA and glucose. In the pH 6.0 medium, the disassembly of the LAMA/AAPBA cross-linking layer led to the highest DOX release from NP_{PrLrB}-DOX.

High biocompatibility is important for a successful drug delivery system. Herein, cell viability and hemolysis

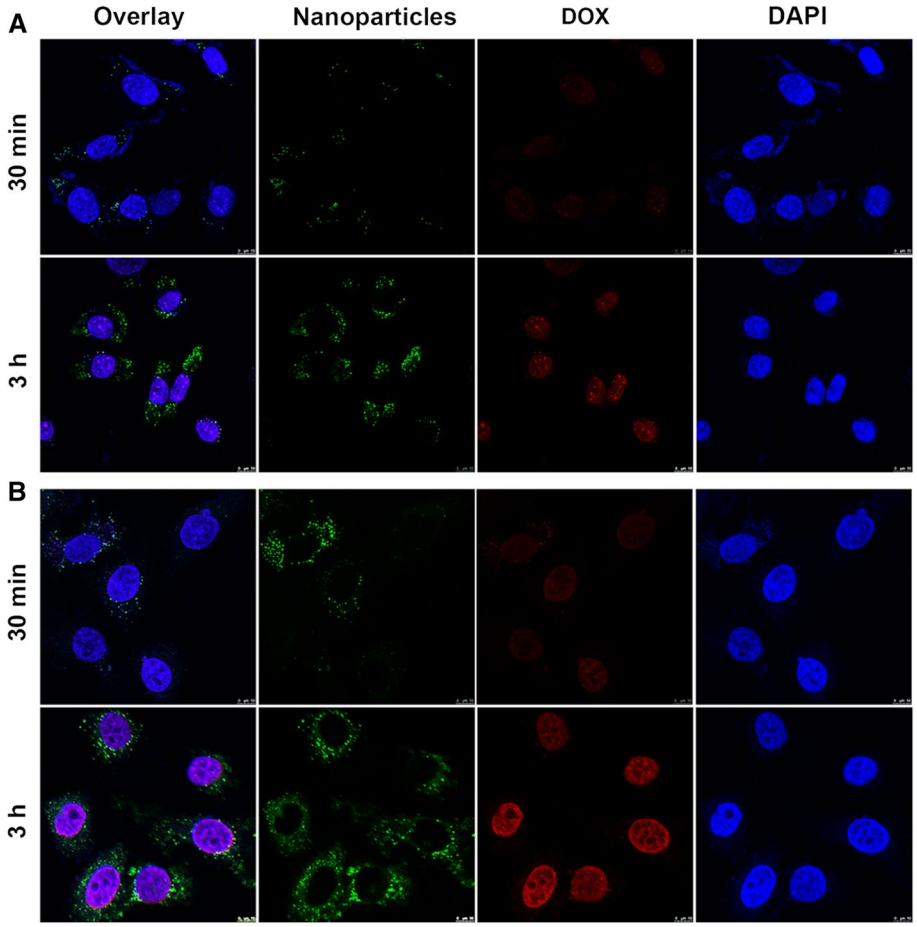

Fig. 3 Cellular uptake of NP_{PrLrB}-DOX: **a** NIH3T3 cells, and **b** HepG2 cells. Nuclei stained with DAPI (blue). DOX (red) released from the nanoparticle (green)

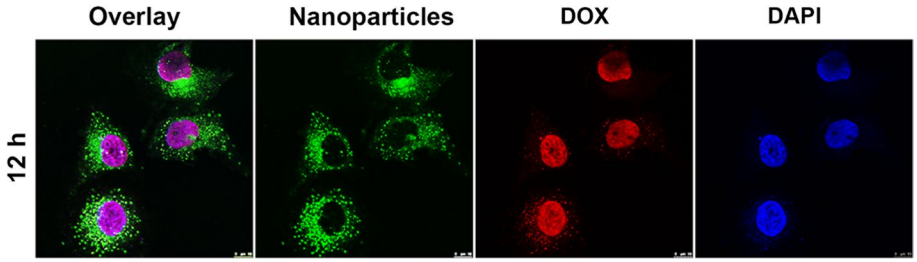

Fig. 4 Cellular uptake after HepG2 cell incubation with NP_{PrLrB}-DOX. Nuclei stained with DAPI (blue). DOX (red) released from the nanoparticle (green)

assays were used to evaluate the cytotoxicity of NP_{PrLrB} (Figs. 2b and c) and NP_{PrLrB}-DOX (Fig. 2d). In Fig. 2b, NP_{PrLrB} showed low cell toxicity with a high concentration of up to 400 µg/mL. In Fig. 2c, hemolysis assay demonstrated a similar result to cell viability, with low hemolysis (< 5%) at high concentrations of NP_{PrLrB}. By contrast, NP_{PrLrB}-DOX exhibited evidently higher cytotoxicity against NIH3T3 and HepG2 cells. NP_{PrLrB}-DOX produced higher cytotoxicity against NIH3T3 cells than HepG2 (Fig. 2d). This difference might result from the targeting activity of LAMA to HepG2. Damaging tumor cells without harming the normal tissues is an important consideration in developing drug delivery systems for the treatment of cancer.

To study drug accumulation in NIH3T3 and HepG2 cells, localization of NP_{PrLrB}-DOX in both cells was observed by confocal microscopy. In Fig. 3, the fluorescent signals in NIH3T3 and HepG2 from NP_{PrLrB} and DOX increased evidently with time. Meanwhile, the fluorescent signals of NP_{PrLrB} and DOX in HepG2 were higher than that of NIH3T3. The fate of NP_{PrLrB}-DOX after internalization was observed by further coincubating it with HepG2 cells for 12 h (Fig. 4). The green fluorescence of NP_{PrLrB} was mainly found in the cytoplasm, and the red fluorescence of DOX

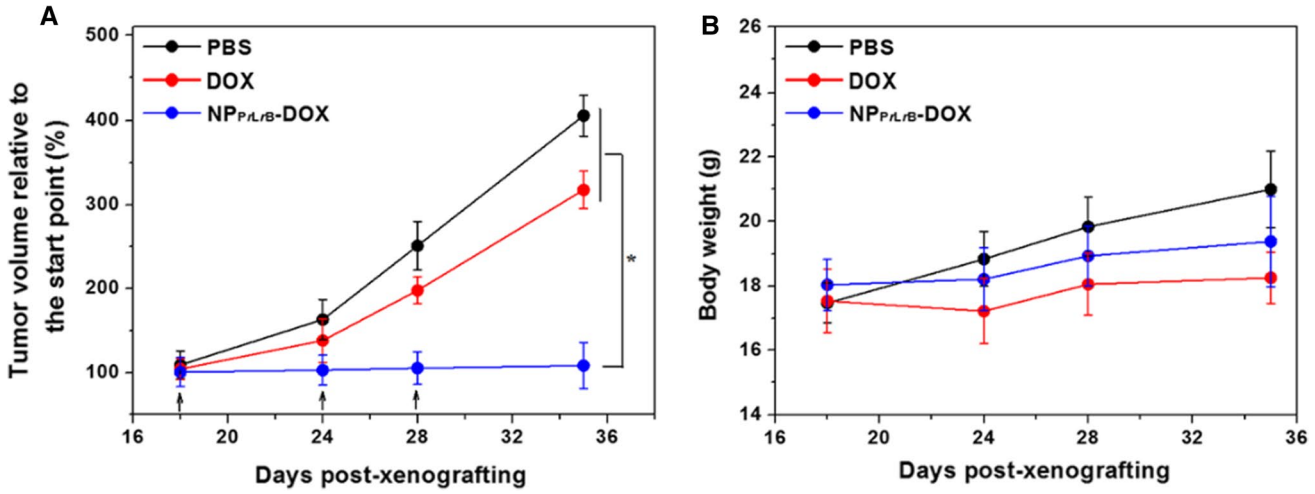

Fig. 5 **a** Inhibition of tumor growth in HepG2 xenograft models after treatment with different agents ($p < 0.05$). **b** Body weight changes in mice after treatment with different agents

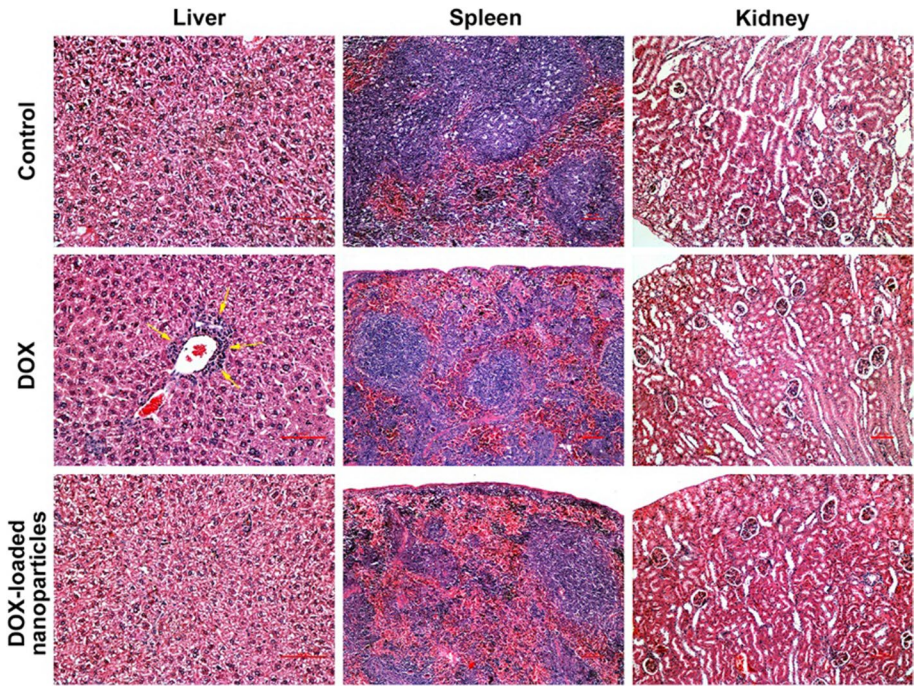

Fig. 6 Histological analysis of H&E-stained liver, spleen, and kidney tissue sections cut from mice, which were treated with PBS, DOX, and NP$_{PrLrB}$-DOX

was mainly detected in the nuclei. These results indicated that NP$_{PrLrB}$-DOX entered the cells, and DOX was successfully released from the nanoparticles and escaped from the lysosomes.

In vivo antitumor assay

We intravenously administrated NP$_{PrLrB}$-DOX to tumor-bearing mice to combat tumor growth effectively, and the antitumor efficacy was studied. Figure 5a shows that tumors grew fast in the PBS group with a threefold increase in volume after 2 weeks. Tumor-bearing mice treated with DOX partly presented an inhibited effect on tumor growth with 2.1-fold increase in tumor volume. In comparison, the tumor-bearing mice treated with NP$_{PrLrB}$-DOX showed evident inhibition of tumor growth with a slight increase in volume over 2 weeks. The limited therapeutic effect of free DOX might be ascribed to its rapid blood clearance and insufficient tumor accumulation. In addition, the body weight of mice was recorded (Fig. 5b), and no obvious body weight loss was found, indicating that the doses of drugs were safe for all the mice.

Generally, DOX in vivo will increase the risk of organ toxicity. T histological analysis was conducted on the main organs, such as the liver, spleen, and kidney, to examine

organ damage. In Fig. 6, multifocal hepatic necrosis and evident inflammatory cells were observed in the livers of mice treated with free DOX. In comparison, no obvious tissue harm was found for mice treated with PBS and NP_{PrLrB}-DOX. No remarkable tissue damages were identified in any spleen and kidney for all the groups.

Conclusions

Herein, a simple and feasible drug self-assembled delivery system with pH responsiveness and targeting function was prepared for cancer therapy. The drug delivery system was composed of DOX and an amphiphilic random copolymer p(AAPBA-*r*-LAMA-*r*-PEGMA) based on phenylboronic acid, galactose, and polyethylene glycol monomethyl ether acrylate molecules by RAFT polymerization. For the polymeric micelles, galactose molecules provided the targeting function for HepG2 cells, while the interaction of phenylboronic acid and galactose supported the pH-responsive behavior. Compared with physiological condition, particle size decreased and morphology changed in an acidic condition, as indicated by the results of DLS and TEM, respectively. Drug-loaded micelles were internalized using HepG2 and NIH3T3 cells, and more drug and micelles were present in HepG2 cells than in NIH3T3 cells. In vivo antitumor assay showed that the drug-loaded micelles significantly inhibited tumor growth with minimal injury to normal tissues. All the results indicated that the synthesized micelles may facilitate the development of valid drug delivery systems for cancer therapy.

Acknowledgements This work was supported by Effect of serum exosome circ-RPPH1 on paclitaxel resistance of breast cancer and its mechanism.

References

Alexander JL, Wilson ID, Teare J, Marchesi JR, Nicholson JK, Kinross JM (2017) Gut microbiota modulation of chemotherapy efficacy and toxicity. Nat Rev Gastroenterol Hepatol 14(6):356

An J, Dai X, Wu Z, Zhao Y, Lu Z, Guo Q, Zhang X, Li C (2015) An acid-triggered degradable and fluorescent nanoscale drug delivery system with enhanced cytotoxicity to cancer cells. Biomacromol 16(8):2444

Arouri A, Hansen AH, Rasmussen TE, Mouritsen OG (2013) Lipases, liposomes and lipid-prodrugs. Curr Opin Coll Interface ence 18(5):419

Ashwell G, Harford J (1982) Carbohydrate-specific receptors of the liver. Annu Rev Biochem 51(1):531

Becker S, Spiess M, Klenk HD (1995) The asialoglycoprotein receptor is a potential liver-specific receptor for Marburg virus. J Gen Virol 76(Pt 2):393

Bray F, Ferlay J, Soerjomataram I, Siegel RL, Torre LA, Jemal A (2018) Global cancer statistics 2018: GLOBOCAN estimates of incidence and mortality worldwide for 36 cancers in 185 countries. CA Cancer J Clin 68(6):394

Cheng C, Zhang X, Wang Y, Sun L, Li C (2012) Phenylboronic acid-containing block copolymers: synthesis, self-assembly, and application for intracellular delivery of proteins. New J Chem 36(6):1413

Cheng W, Nie J, Xu L, Liang C, Peng Y, Liu G, Wang T, Mei L, Huang L, Zeng X (2017) pH-sensitive delivery vehicle based on folic acid-conjugated polydopamine-modified mesoporous silica nanoparticles for targeted cancer therapy. ACS Appl Mater Interfaces 9(22):18462

Cheng YJ, Qin SY, Ma Y, Chen XS, Zhang AQ, Zhang XZ (2019) Super-pH-sensitive mesoporous silica nanoparticles-based drug delivery system for effective combination cancer therapy. ACS Biomater Sci Eng 5:1878

Chen H, Liu Z, Wei B, Huang J, You X, Zhang J, Yuan Z, Tang Z, Guo Z, Wu J (2021) Redox responsive nanoparticle encapsulating black phosphorus quantum dots for cancer theranostics. Bioactive Mater 6(3):655

Cho K, Wang X, Nie S, Chen ZG, Shin DM (2008) Therapeutic nanoparticles for drug delivery in cancer. Clin Cancer Res 14(5):1310

Duan Q, Cao Y, Li Y, Hu X, Xiao T, Lin C, Pan Y, Wang L (2013) pH-responsive supramolecular vesicles based on water-soluble pillar[6]arene and ferrocene derivative for drug delivery. J Am Chem Soc 135(28):10542

Duan X, Chen H, Fan L, Kong J (2016) Drug self-assembled delivery system with dual responsiveness for cancer chemotherapy. ACS Biomater Ence Eng 21:2347

Fallon RJ, Schwartz AL (1988) Asialoglycoprotein receptor phosphorylation and receptor-mediated endocytosis in hepatoma cells Effect of phorbol esters. J Biol Chem 263(26):13159

Fang S, Niu Y, Zhu W, Zhang Y, Yu L, Li X (2015) Liposomes assembled from a dual drug-tailed phospholipid for cancer therapy. Chem Asian J 10(5):1232

Gao X, Zhai M, Guan W, Liu J, Liu Z, Damirin A (2017) Controllable synthesis of a smart multifunctional nanoscale metal-organic framework for magnetic resonance/optical imaging and targeted drug delivery. ACS Appl Mater Interfaces 9(4):3455

Guo Q, Wang Y, Zhang L, Zhang P, Yu Y, Zhang Y, Li C, Jiang S, Zhang X (2019) In situ real-time tracing of hierarchical targeting nanostructures in drug resistant tumors using diffuse fluorescence tomography. Chem Sci 10(34):7878

Han Y, Yin W, Li J, Zhao H, Zha Z, Ke W, Wang Y, He C, Ge Z (2018) Intracellular glutathione-depleting polymeric micelles for cisplatin prodrug delivery to overcome cisplatin resistance of cancers. J Control Release: Official J Control Release Soc 273:30

Hashida M, Nishikawa M, Yamashita F, Takakura Y (2001) Cell-specific delivery of genes with glycosylated carriers. Adv Drug Deliv Rev 52(3):187

He L, Read ES, Armes SP, Adams DJ (2007) Direct synthesis of controlled-structure primary amine-based methacrylic polymers by living radical polymerization. Macromolecules 40(13):4429

Koyamatsu Y, Hirano T, Kakizawa Y, Okano F, Takarada T, Maeda M (2014) pH-responsive release of proteins from biocompatible and biodegradable reverse polymer micelles. J Control Release: Official J Control Release Soc 173:89

Lee MC, Kabilan S, Hussain A, Yang X, Blyth J, Lowe CR (2004) Glucose-sensitive holographic sensors for monitoring bacterial growth. Anal Chem 76(19):5748

Lepenies B, Lee J, Sonkaria S (2013) Targeting C-type lectin receptors with multivalent carbohydrate ligands. Adv Drug Deliv Rev 65(9):1271

Lin X, Li AM, Li YH, Luo RC, Zou YJ, Liu YY, Liu C, Xie YY, Zuo S, Liu Z et al (2020) Silencing MYH9 blocks HBx-induced

GSK3β ubiquitination and degradation to inhibit tumor stemness in hepatocellular carcinoma. Signal Transduct Target Ther 5(1):13
Li Y, Xiao W, Xiao K, Berti L, Luo J, Tseng HP, Fung G, Lam KS (2012) Well-defined, reversible boronate crosslinked nanocarriers for targeted drug delivery in response to acidic pH values and cis-diols. Angewandte Chemie (Int ed in English) 51(12):2864
Li M, Song W, Tang Z, Lv S, Lin L, Sun H, Li Q, Yang Y, Hong H, Chen X (2013) Nanoscaled poly(L-glutamic acid)/doxorubicin-amphiphile complex as pH-responsive drug delivery system for effective treatment of nonsmall cell lung cancer. ACS Appl Mater Interfaces 5(5):1781
Li X, Wang X, Sha L, Wang D, Shi W, Zhao Q, Wang S (2018) Thermosensitive lipid bilayer-coated mesoporous carbon nanoparticles for synergistic thermochemotherapy of tumor. ACS Appl Mater Interfaces 10(23):19386
Pan J, Li PJ, Wang Y, Chang L, Wan D, Wang H (2018) Active targeted drug delivery of MMP-2 sensitive polymeric nanoparticles. Chem Commun (Camb) 54(79):11092
Saw PE, Xu X, Zhang M, Cao S, Farokhzad OC, Wu J (2020) Nanostructure engineering by simple tuning of lipid combinations. Angewandte Chemie (Int ed in English) 59(15):6249
Su J, Chen F, Cryns VL, Messersmith PB (2011) Catechol polymers for pH-responsive, targeted drug delivery to cancer cells. J Am Chem Soc 133(31):11850
Tan YF, Lao LL, Xiong GM, Venkatraman S (2018) Controlled-release nanotherapeutics: state of translation. J Control Release: Off J Control Release Soc 284:39
Wang H, Lu Z, Wang L, Guo T, Wu J, Wan J, Zhou L, Li H, Li Z, Jiang D et al (2017b) New generation nanomedicines constructed from self-assembling small-molecule prodrugs alleviate cancer drug toxicity. Can Res 77(24):6963
Wang H, Wu J, Xu L, Xie K, Chen C, Dong Y (2017a) Albumin nanoparticle encapsulation of potent cytotoxic therapeutics shows sustained drug release and alleviates cancer drug toxicity. Chem Commun (Camb) 53(17):2618
Yao C, Wang P, Li X, Hu X, Hou J, Wang L, Zhang F (2016) Near-infrared-triggered azobenzene-liposome/upconversion nanoparticle hybrid vesicles for remotely controlled drug delivery to overcome cancer multidrug resistance. Adv Mater (Deerfield Beach, Fla) 28(42):9341
Zhang P, Wang Y, Lian J, Shen Q, Wang C, Ma B, Zhang Y, Xu T, Li J, Shao Y et al (2017b) Engineering the surface of smart nanocarriers using a pH-/Thermal-/GSH-responsive polymer zipper for precise tumor targeting therapy in vivo. Adv Mater (Deerfield Beach, Fla) 29:36
Zhang Z, Shi L, Wu C, Su Y, Qian J, Deng H, Zhu X (2017a) Construction of a supramolecular drug-drug delivery system for non-small-cell lung cancer therapy. ACS Appl Mater Interfaces 9(35):29505
Zhang M, Song CC, Su S, Du FS, Li ZC (2018) ROS-activated ratiometric fluorescent polymeric nanoparticles for self-reporting drug delivery. ACS Appl Mater Interfaces 10(9):7798
Zhang M, Ma Y, Wang Z, Han Z, Gao W, Zhou Q, Gu Y (2019) A CD44-targeting programmable drug delivery system for enhancing and sensitizing chemotherapy to drug-resistant cancer. ACS Appl Mater Interfaces 11(6):5851